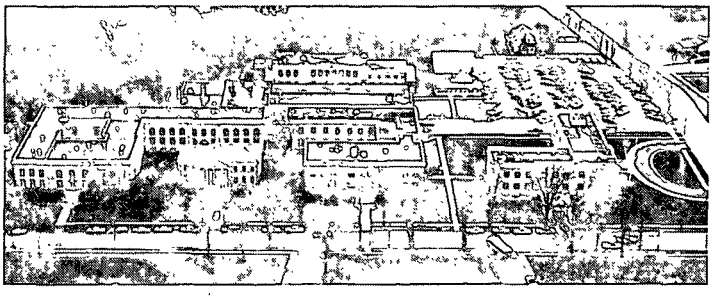

THE INSTITUTE OF PAPER CHEMISTRY, APPLETON, WISCONSIN

IPC TECHNICAL PAPER SERIES

NUMBER 330

THE PHYSICS OF IMPULSE DRYING: NEW INSIGHTS FROM NUMERICAL MODELING

J. D. LINDSAY

MARCH, 1989

The Physics of Impulse Drying: New Insights from Numerical Modeling

J. D. Lindsay

This manuscript is based on results obtained in IPC research and is to be presented at the Ninth Fundamental Research Symposium in Cambridge, England, on September 16-22, 1989

The Physics of Impulse Drying: New Insights from Numerical Modeling

J. D. Lindsay
The Institute of Paper Chemistry
Appleton, Wisconsin

ABSTRACT

In order to better understand the physics of impulse drying, two numerical models have been developed to predict the transient heat transfer, vapor pressure development, and vapor-liquid flow during impulse drying. The first model, MIPPS-I, examines impulse drying as a moving boundary problem in which a sharp front of steam displaces a saturated liquid phase. While several key insights were obtained with this approach, a comparison of predictions with experimental data suggested that the sharp-interface assumption should be abandoned in favor of a two-phase zone between the dry and saturated regions. A new model, MIPPS-II, was then developed which allows a two-phase zone to develop. Both models use finite-difference forms of the mass, momentum, and energy conservation equations adapted for porous media.

Analysis of the numerical results in light of experimental data helps clarify some of the transport processes in impulse drying. In particular, it appears that the impulse drying process depends on the continued boiling of liquid near the hot surface with condensation occurring in the cooler, more saturated regions. The process of boiling and condensation is tied to sheet permeability and pore structure. The liquid for

sustained boiling is available in saturated dead-end pores or is supplied by capillary flow.

The numerical results show that the development of an internal vapor zone is critical to several features of the impulse drying process. The pressurized vapor zone enhances water removal through direct displacement and also possibly by reducing or eliminating rewet. Relationships between sheet properties and internal vapor pressure and water removal can now be better understood with the aid of the models.

Several new pieces of experimental information are also presented which have guided recent model developments and, at the same time, can be interpreted in terms of results from the models. The new experimental data include flash x-ray visualization of interface motion in impulse drying and several measurements of thermal processes in both paper and model fibrous porous media.

INTRODUCTION

Impulse drying is a novel water removal process which was first developed at The Institute of Paper Chemistry. At a superficial level, impulse drying can be described as a simple variation of wet pressing, with one roll heated to 250-375°C (Figure 1). (When commercialized, practical systems may use a long-nip press with a heated roll.) In impulse drying, intense heat transfer interacts with other mechanisms to create a process that gives significantly higher dryness than wet pressing while using less energy than conventional cylinder drying. Impulse drying not only offers the potential for energy and capital savings over traditional dewatering and drying methods, but can give significantly improved paper properties as well (1-3).

While the key to impulse drying is believed to be the creation of a vapor phase within the sheet, conflicting theories have been advanced, and even where there is consensus, much remains poorly understood. In order to overcome the remaining roadblocks to industrial implementation of impulse drying, our physical understanding must be advanced. The difficulty of directly observing transport processes inside the nip, combined with uncertainties in interpreting experimental data, suggest that new tools are needed to supplement

experimental studies. Numerical modeling is such a tool. While modeling cannot replace observation, it can greatly enhance it. Ideally, the combined application of modeling and observation should lead to insights not available with either approach alone.

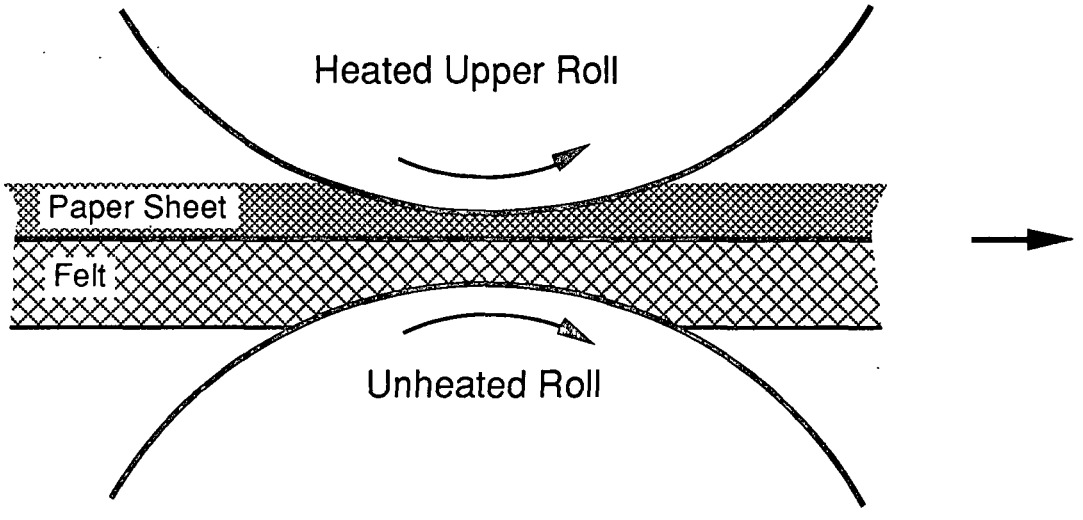

Figure 1. The impulse drying concept.

The objective of this paper is to apply computational tools to further our understanding of the impulse drying process. The process is cyclical: experimental information about a process is needed in order to give the modeler an idea of what processes must be modeled. The key equations and assumptions must then be chosen and formulated in a framework to permit numerical solution. The resulting numerical model can be evaluated in light of experimental data, and the data can be interpreted in light of the model, if the model proves to be "reasonable" or "useful." Skepticism is always healthy, both toward the numerical predictions and the experimental data. With this in mind, let us first review some of the key experimental observations (and hypotheses of experimentalists) about impulse drying before proceeding with the model derivation.

OVERVIEW OF IMPULSE-DRYING PHYSICS

Thermally-driven Displacement

The results of previous studies over the past several years have done much to characterize the impulse drying process (1-4). The basic features of impulse drying are now well known: intense heat transfer, rapid water removal, high energy efficiency compared to conventional drying, and densification similar to that of wet pressing.

Based on their analysis of the experimental data, several researchers (2,4,5) have concluded that impulse drying relies on the creation of a vapor phase which helps to remove the free liquid in the sheet. While in the nip, vapor apparently forms in the sheet next to the hot surface, as shown in Figure 2. The sustained hydraulic pressure from the vapor zone may help to drive liquid water out of the sheet into the felt below. Since most of the water is removed as a liquid in such a displacement process, the energy efficiency would be high.

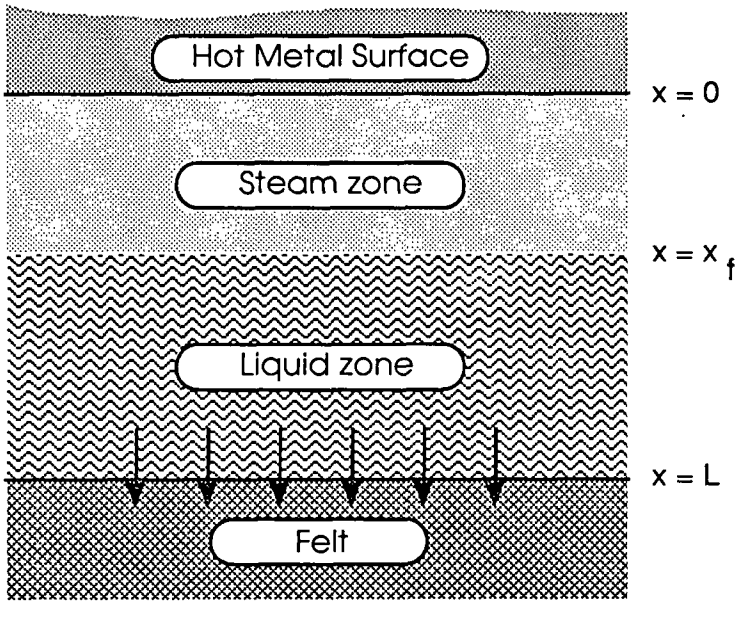

Figure 2. A one-dimensional displacement view of impulse drying.

In this view of impulse drying, intense heat transfer is needed to maintain a high vapor pressure which provides the driving force for the removal of water beyond what is possible with regular wet pressing. Naturally, some of the mechanisms of hot pressing (viscosity reduction, softening of fibers) also come into play, but significant vapor-liquid displacement is one of the key factors which distinguish impulse drying from conventional processes.

Because impulse drying can be described as wet pressing with a heated roll, the relation of impulse drying to other processes such as wet pressing and hot pressing has been a source of some confusion and speculation. These relationships have now been at least partially clarified by Sprague (5), who provides a new unifying framework. His analysis highlights the unique characteristics of impulse drying, which cannot be viewed as simply a combination of evaporative drying and pressing. The importance of a unique heat transfer mechanism in impulse drying is thus strengthened.

Heat Transfer

The heat transfer rate is a critical factor in the physics of impulse drying. An example of a measured heat flux during impulse drying is given in Figure 3, adapted from the thesis of Burton (2). Burton used temperature data from a thermocouple mounted in the heated head of a falling-weight press-nip simulator to calculate the flux into the sheet. Many similar measurements (1,4) tend to show the general features of Figure 3: a rapid rise in heat flux to a peak near midnip, followed by a decline. Peak heat fluxes can range from 1 to 8 MW/m^2, and measurements have shown that sustained heat flux values on the order of 0.5 to 1.5 MW/m^2 are possible for 100 milliseconds or more after the peak, if the mechanical pressure is maintained. Sustained heat fluxes of this magnitude imply a continuing phase-change process.

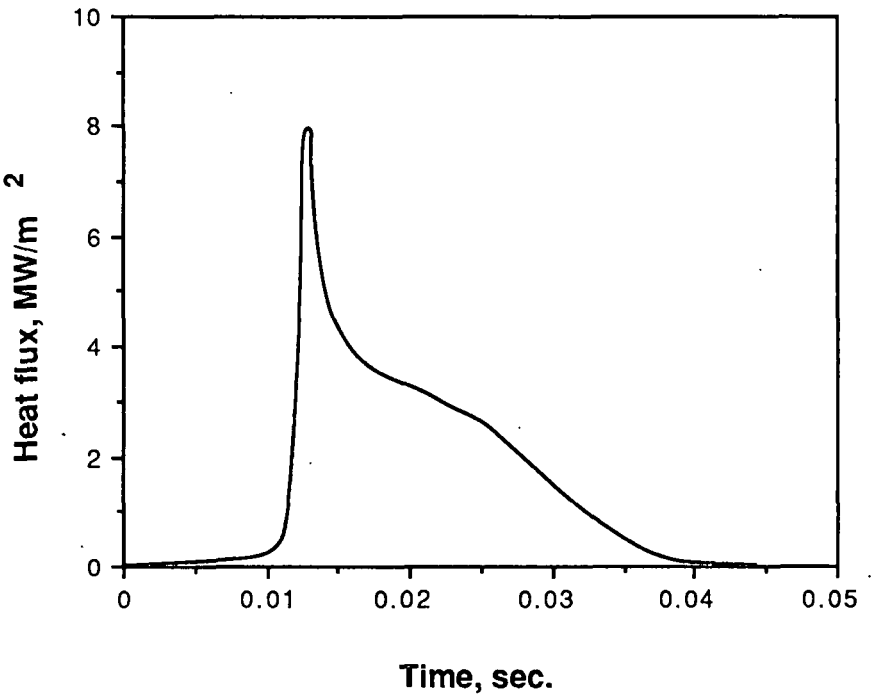

Figure 3. Transient heat flux during an impulse drying event . Measurement was made by Burton (2) with a falling-weight press-nip simulator.

The observed heat transfer rates in impulse drying may be evidence of a complex heat-pipe mechanism. A heat pipe is a heterogeneous heat transfer device in which fluid is wicked through a porous medium from a cool to a hot region by capillary forces, whereupon the liquid boils into a void region (6). The hot vapor then flows to the low-pressure cool zone to be condensed. Sonic velocities in the vapor phase can be achieved in some cases. The process of boiling and condensation allow heat to be transferred rapidly across large distances, greatly increasing the apparent thermal conductivity of the system.

In impulse drying, small capillaries with high capillary pressures may act as conduits for liquid to flow against a gas pressure gradient back to the hot surface, where it can boil and flow through the larger pores back toward the cooler saturated zone. A similar mechanism has already been observed

in the cylinder drying of paper (7). Such a process would allow boiling heat transfer to take place over a long period of time even though most of the liquid might be well removed from the hot surface. This possibility will be considered in the modeling work below.

Vapor Pressure Development and Delamination

A challenging problem which has slowed the commercial development of impulse drying is delamination. Unfortunately, in some cases the vapor zone can develop pressures great enough to rupture or delaminate the sheet as it leaves the nip. Delamination is probably related to the blistering which can occur in the drying of coated papers with low surface porosity in which internally released steam builds up enough pressure to overcome z-direction bonding (8).

In furnishes where delamination may be a problem, it can be prevented if the nip residence time is long enough for the vapor to remove the water seal on the felt side, or if the rate of heat transfer can be controlled in some way such that the internal vapor pressure does not exceed the sheet strength (9). Much remains uncertain. An improved understanding of heat transfer mechanisms may be especially important if the delamination problem is to be more fully tamed.

INSIGHTS FROM NEW EXPERIMENTAL WORK

Recent experimental data from ongoing studies of impulse drying physics conducted at The Institute of Paper Chemistry provide new information beyond what has been previously published. Because the implications of these studies have relevance to the modeling work, some of the new data will be briefly discussed here.

Flash X-ray Visualization

In an effort to visualize the steam-water interface in impulse drying, Zavaglia and Lindsay (10) have used flash x-ray radiography to track the motion of an x-ray-absorbing silver nitrate tracer solution added to the upper layers of a linerboard sheet. Impulse drying and wet pressing events were approximated with a falling-weight press-nip simulator. During the pressing event, a brief burst of x-rays was sent

horizontally through the sheet and the felt, as shown in Figure 4. The location of the silver nitrate solution in the z-direction could be observed in the radiograph. Different delay times are used in each run, allowing fluid motion to be observed in time.

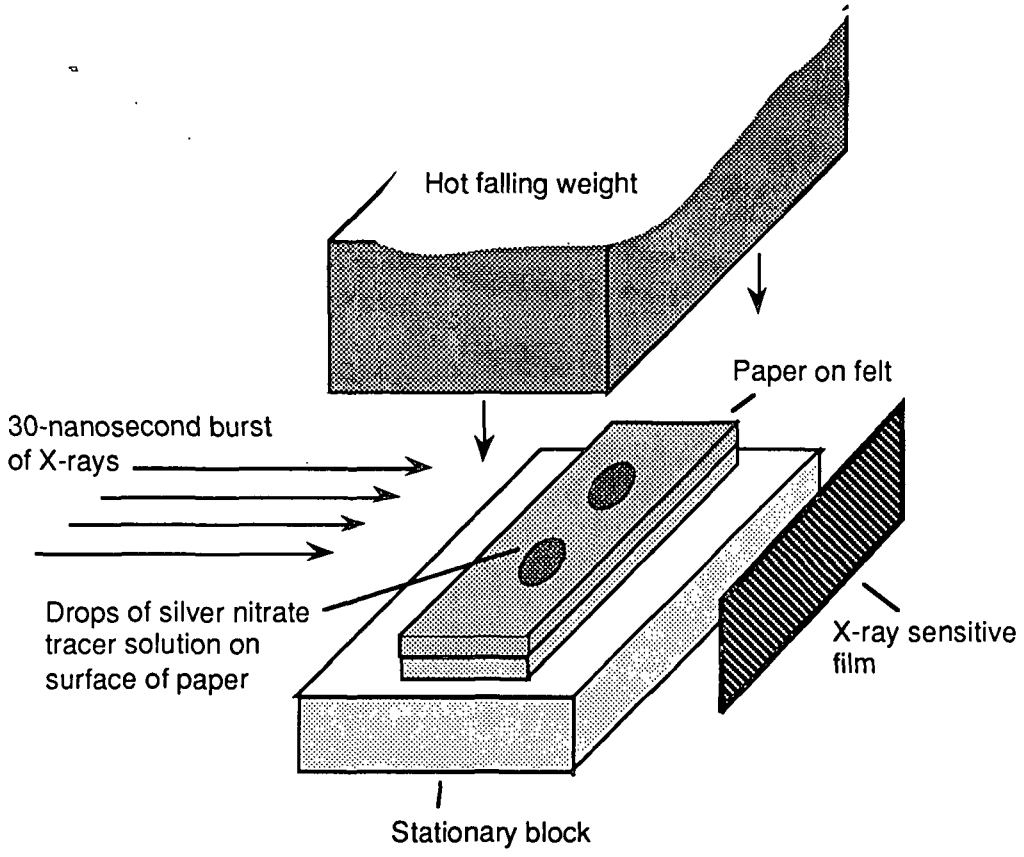

Figure 4. Experimental configuration for flash x-ray visualization of liquid motion in impulse drying. The location of tracer solution in the vertical direction can be viewed during any part of a pressing event.

Figure 5 shows radiographs taken of events under wet-pressing and impulse-drying conditions; the only difference between the two runs was the high surface temperature (250°C) of the falling weight in the impulse drying case. In the wet pressing case, the silver nitrate solution in the upper layers of the sheet has spread in the z-direction, and some of the

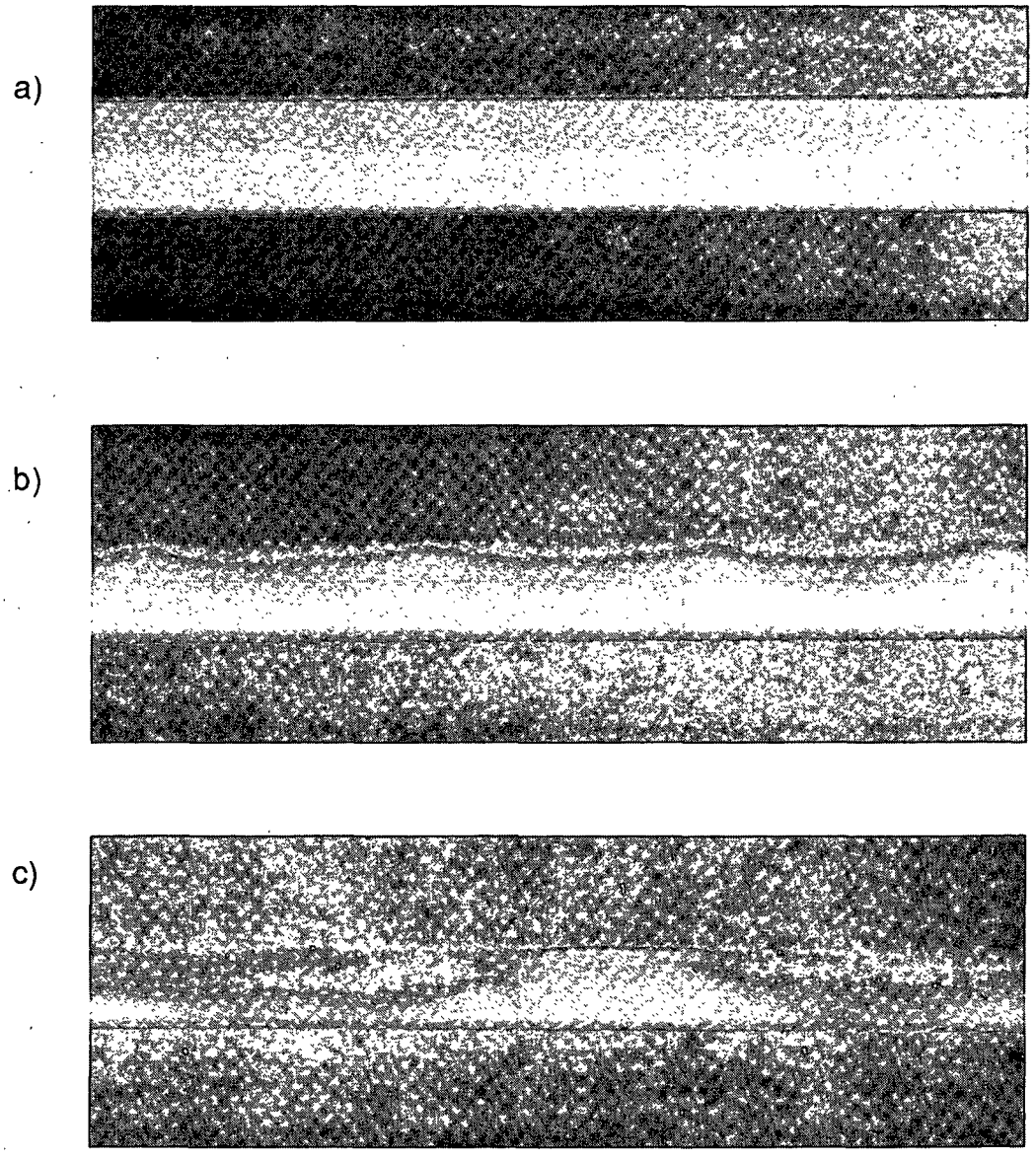

Figure 5. Flash x-ray radiographs of wet pressing and impulse drying events in linerboard on a felt in a falling-weight press-nip simulator. Top photo (a) shows an impulse drying event without tracer solution present. Middle photo (b) shows a wet-pressing event with silver nitrate tracer solution initially present as drops on the upper surface of the paper. Bottom photo (c) shows an impulse drying event with tracer solution under the same conditions as in (b) except the head temperature is 245°C.

Typical results are shown in Figure 6, where the peak pressure is varied from 600 to 1600 psi. The water removal data are reported as mass of water removed divided by the initial sheet weight. The difference between the wet pressing and impulse drying curves represents the extra water removed by impulse drying. Interestingly, the amount of extra water removed does not seem to decrease with increasing pressure over the range investigated. The results of Figure 6 were replicated in two other batches of handsheets, and the same trend was also observed over the pressure range of 200-600 psi in other linerboard handsheets.

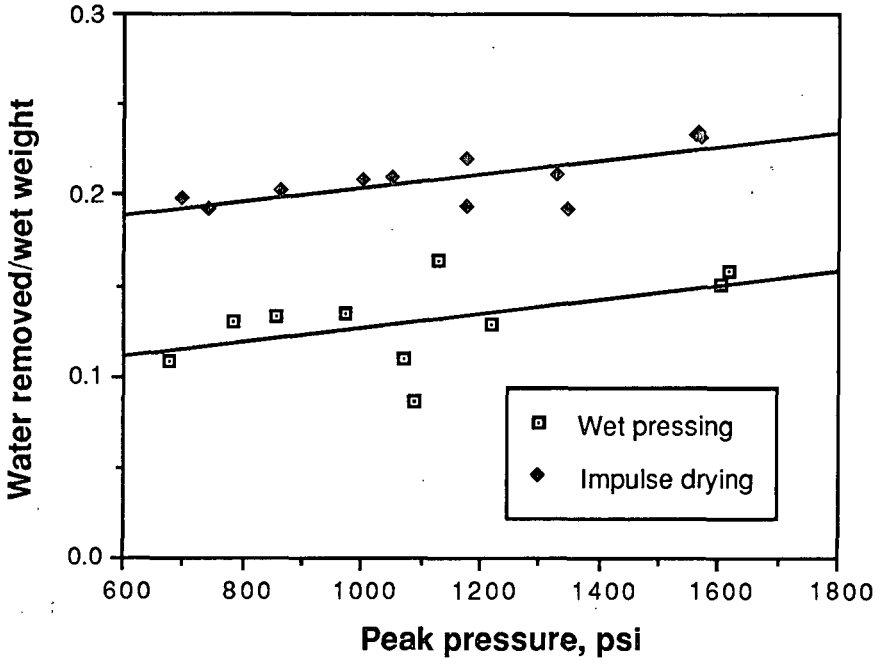

Figure 6. Comparison of water removal in wet pressing and impulse drying as a function of pressure. 250g/m^2 linerboard handsheets were used. Impulse drying temperature was 260 °C.

The extra water removed by impulse drying would be constant if it were all due to vaporization, but the measurements of water added to the felt show that about 90% of the extra water removed is in liquid form (the possibility of steam breaking through the 250 g/m^2 sheet and condensing in the felt is easily ruled out by an examination of felt surface temperature in

related measurements). This is consistent with the energy balance and mass balance measurements made by Lavery (1,4), and contradicts a recent speculation (12) that the heat flux into the sheet simply provides energy to evaporate the water, and that the gain of impulse drying over wet or hot pressing is due to evaporative removal alone.

The small pressure-dependency in the extra water removed by impulse drying may be due to several factors compensating each other, as discussed above. But it also raises the possibility that a mechanism with less pressure dependency than displacement may be contributing to the extra water removal found in impulse drying. Such a mechanism might be rewet reduction, as discussed below.

Rewet Reduction by Impulse Drying

The modeling results presented in this paper along with the physical observation of delamination both suggest that significant vapor pressures can exist throughout the entire pressing event, and that these pressurized vapor zones are not just confined to the upper surface of the sheet. With a pressurized vapor region already in the sheet, the normal process of rewet may be greatly reduced or reversed in impulse drying. This contribution to liquid water removal in impulse drying has apparently not been considered before, but may be of importance. The hypothesis is thus advanced that the enhanced liquid water removal obtained in impulse drying is indeed due to the presence of a pressurized vapor phase, but that the mechanism must include both displacement and rewet reduction. The pressurized vapor zone is expected to reduce rewet by suction, capillary forces, and film splitting. Student research on this possibility is currently underway (13).

Temperature History

Measurement of local temperature histories within a sheet provides useful information. Burton reported a measurement of internal sheet temperatures at three different layers inside a linerboard sheet during a simulated impulse drying event (2). In spite of uncertainties in the data and its interpretation, the temperature history in each layer appears to be consistent with a displacement model of impulse drying, and could be interpreted as evidence that a distinct steam-liquid interface was moving through the sheet. Only recently have much more

extensive measurements of internal temperature propagation become available as part of a study by Sprague (5). The results require some rethinking about impulse drying processes.

Sprague used stacks of thin, wet sheets of bleached kraft paper, each sheet having a basis weight of 50 g/m^2. Extremely thin thermocouples were sandwiched between the layers. During impulse drying with the MTS electrohydraulic press simulator, the temperature at each layer (including the felt-sheet interface) could be tracked in time. Tests showed that temperature propagation through a stack of thin sheets was essentially the same as temperature propagation through a single thicker sheet with the same cumulative basis weight, indicating that interface effects between the sheets were of minor concern.

Sample results are presented in Figures 7 and 8. Figure 7 shows the temperature at the felt-paper interface beneath a single 50 g/m^2 sheet. Three thermocouples at different locations on that interface were used, two of which gave nearly identical results; a significantly different third curve may have been due to a thermocouple problem or may be an indication of real nonuniformities. The upper two curves show traits found in several of the measurements: a steep S-shaped rise to a plateau above the ambient boiling temperature, followed by a rapid temperature rise which then levels off.

Measurements at three transverse locations are shown in Figure 8, where somewhat different trends can be seen. Here three 50 g/m^2 sheets have been stacked, and single thermocouples have been placed between the sheets. The upper curve from the thermocouple closest to the surface does not show an intermediate plateau as in Figure 7. The second curve, showing data from the interface between the middle and bottom sheets, does show an S-shaped rise followed by a nearly flat region. The thermocouple at the sheet-felt interface shows only a gradual temperature rise.

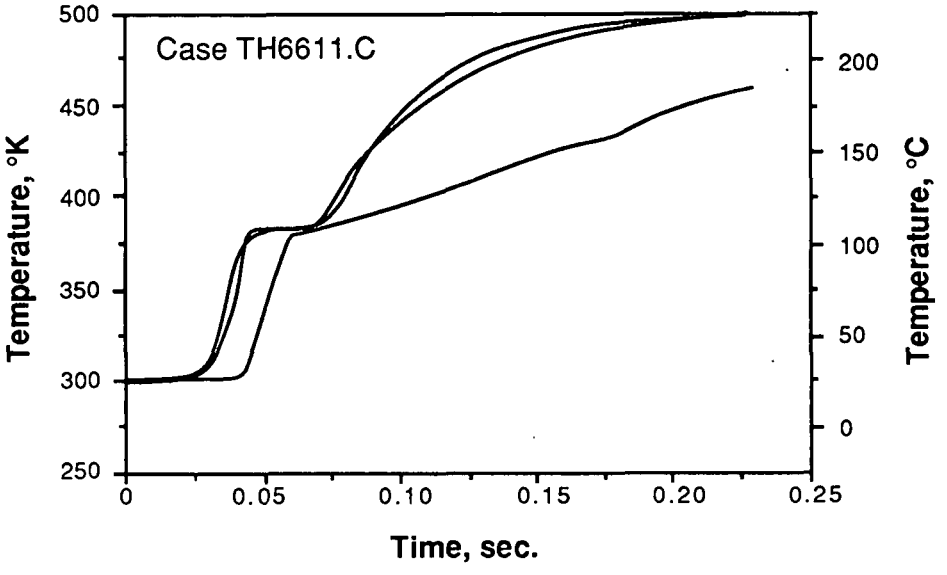

Figure 7. Temperature propagation at the backside of a 50 g/m^2 sheet impulse dried with a head temperature of 530°K. Three thermocouples were placed on the paper-felt interface.

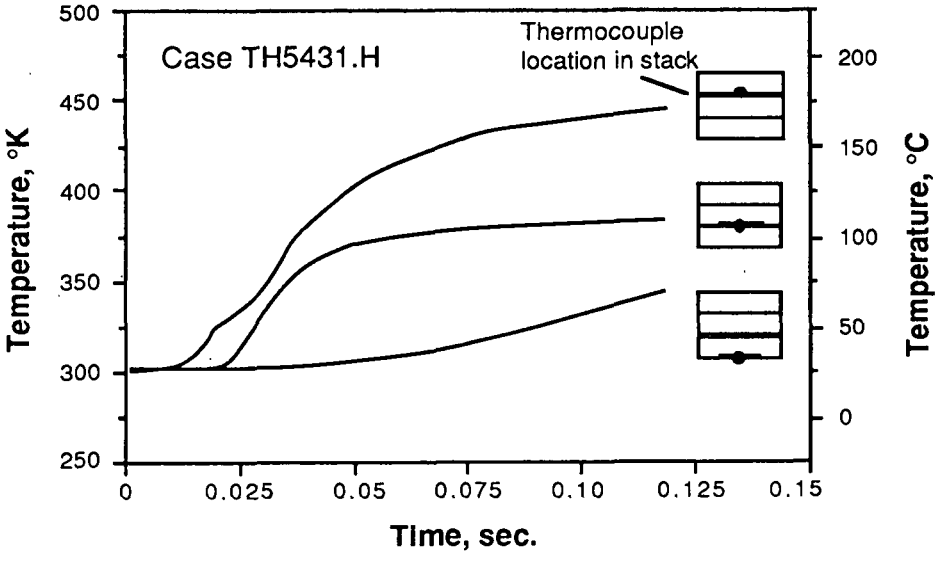

Figure 8. Temperature propagation at the inter-layer locations of a stack of three 50 g/m^2 sheets impulse dried with a head temperature of 260° C (530° K). Sheets lie on a felt.

The above results can be interpreted in terms of the vapor-liquid displacement concept. The existence of plateau regions somewhat above 100°C is strong evidence for a two-phase zone where the vapor and liquid are in equilibrium at an elevated pressure. The two-phase zone at any point may only be temporary, and as it is displaced or evaporated, a dry zone with higher temperatures follows. In some cases, the two-phase zone is very thin (or nonexistent), so a sharp steam-water interface may be a good description of the process. Regions of slow temperature rise, such as the bottom curve in Figure 8 or the initial period of the S-shaped regions during the first few milliseconds of impulse drying, show the effect of transient conduction heating through a saturated liquid zone. In short, the data are consistent with the proposed displacement mechanism of impulse drying, and provide new evidence that extended two-phase zones may be formed during impulse drying. (The interpretation of these recent data has been aided by an examination of the numerical results from this study.)

Another recent experimental study of impulse drying in fiberglass sheets will be briefly discussed in conjunction with modeling results below.

The experimental information reviewed above provides a framework for model development and evaluation. After a brief review of related modeling efforts, we can present the modeling approaches of this study.

PREVIOUS NUMERICAL STUDIES

While numerical heat transfer studies of complex processes abound in the engineering literature, the only prior numerical investigation of impulse drying is found in a thesis by Pounder (14). Pounder began with a two-zone model of displacement from Ahrens (15), and extended it to a four-zone model including mat compressibility. The resulting model gave insight into the complexity of the impulse drying process and represented an ambitious first step in impulse drying modeling. While some aspects of the model are clearly successful (the incorporation of sheet compression, for instance), the treatment of the different zones seems to have resulted in a number of unrealistic predictions characterized by periods of linear change in time punctuated with discontinuities (occasionally large spikes) during the transition from one regime to another. Predicted heat transfer rates in particular did not compare

well with observation. There may have been deficiencies in the numerics as well as in the assumed physics of the process.

Several models of conventional paper drying have also been published (e.g.,16,17), but this process is significantly different from impulse drying. Ahrens has developed analytical models for vacuum drying (18) and displacement dewatering (15) which highlight the importance of two-phase flow processes.

A number of related numerical studies outside of the paper industry have been published. A good review of two-phase flow modeling in soil is given by Milly (19), where some of the challenges of such modeling are shown. Soil hydrology is generally unconcerned with heat transfer effects, although Pollock treated two-phase flow and heat transfer in a model concerned with radioactive effluents (20). Displacement processes for the petroleum industry have frequently been modeled (21-23), but these provide little direct assistance for the problem at hand. Models of heat pipes have been developed which are of relevance in understanding some heat transfer effects, although simultaneous displacement is not considered (24).

Moving Boundary Models

Phase-change problems in which a phase boundary moves have received much attention recently. This class of moving boundary problems requires unique and difficult solution methods [see (25) for a review]. Analytical solutions are available only for the simplest cases, and may be impossible when physical properties change with temperature. Such problems occur in many diverse areas, including ablation of heat shields in spacecraft, melting of permafrost, and the melting and solidification of alloys [several examples are treated in (26)]. In impulse drying, the vapor-liquid boundary moves not only because of phase-change but also because the liquid is driven out by the generated vapor pressure. Impulse drying is thus related to another set of moving boundary problems involving phase displacement in porous media.

In general, moving boundary problems require the simultaneous numerical solution of transport equations in two distinct phases which are coupled through boundary conditions at the moving phase boundary. The location of the interface is not known *a priori*, so iterative procedures are usually

required. Both finite-element and finite-difference techniques have been used. One-dimensional problems are most commonly treated, although many recent studies have been published with two and even three-dimensional solutions (27,28). Because of the numerical difficulties in treating a sharp interface, approximations are often employed with a "mushy" zone separating the phases (29), but this approach will be avoided here.

MODEL DEVELOPMENT: MIPPS-I

Model Assumptions

In MIPPS-I, impulse drying is treated as a moving boundary problem with a sharp vapor-liquid interface. The two phases are joined through boundary conditions that apply only at the interface. Conservation equations for heat, mass, and momentum are applied simultaneously to both phases in such a way that the changing boundary conditions at the interface are constantly satisfied.

The combination of pressure-driven displacement and phase-change heat transfer makes the impulse drying process an unusual and complex moving boundary problem. Furthermore, contrary to the assumption made in virtually all past studies of moving boundary problems with phase-change, the interface pressure and temperature are not constant but vary significantly with time.

To avoid excessive complexity in the model, the paper is treated as rigid during the impulse drying process. This assumption can be partially justified by viewing impulse drying as a two-step process consisting of a wet-pressing stage and a vapor-liquid displacement stage. Vapor pressure acts to augment wet pressing once the wet pressing process starts to die down. In wet pressing, peak hydraulic pressures occur before midnip, and are dropping rapidly by midnip (30). The region of interest for the modeling, then, begins with the near-midnip portion of the process in which the sheet has already been compressed and most of the water removal by compression has already occurred. This is consistent with experimental data taken at The Institute of Paper Chemistry showing the intense heat transfer processes of impulse drying are not fully underway until most of the sheet compression has occurred (1,2).

For simplicity, therefore, MIPPS ignores the compression processes early in the nip and assumes that the sheet has been compressed before the thermal processes of impulse drying begin. At this stage, the sheet can be treated as a rigid, homogeneous porous medium. The sheet is assumed to consist of cellulose and water only. Heat transfer during the compression stage has been ignored, and only now does the paper "sense" the hot surface at temperature T_o. (These assumptions would be exact for a truly rigid sheet.) As heat flows into the liquid, a vapor phase forms which forces the free saturated liquid into the felt below (see Figure 2). Because water removal by compression has already occurred, the motion of the vapor zone through the saturated sheet is an indication of additional water removal by displacement in impulse drying.

The assumption of rigidity still introduces error into the model, but the effect of compression should not significantly affect the fundamental physics of the impulse drying process. The effect of transient compression should primarily be a transient change in physical properties and boundary conditions.

Another key but problematic feature in MIPPS-I is the ability for the user to specify a capillary wicking rate for water transported from the saturated zone to the hot surface. This is an *ad hoc* feature which allows the possibility of a heat pipe mechanism to be examined. While this approach is greatly oversimplified, it does allow some wicking effects to be examined. It is problematic because capillary wicking implies that a two-phase zone exists across which the wicking occurs, a possibility excluded by the sharp-interface assumption. If one assumes that the capillary flow occurs only through a few small and perfectly insulated pores, the contradiction can be overlooked. Again, we are modeling a complex system in a simplistic way with the hope of understanding a little more than when we began. The sophistication of the model must proceed in steps.

Formulation of the Conservation Equations

Because of the complexity of porous media, it is impossible to model transport processes at the microscopic level. Instead, the porous medium is treated as if it were a continuum by averaging microscopic transport laws over a characteristic volume of the porous medium (31,32). Complex tensor relationships with dozens of empirical terms may result which are then simplified to tractable forms by a combination of dimensional analysis, heuristic reasoning, and pure faith. As a result, there is always a degree of uncertainty, empiricism, and perhaps even confusion in any so-called "fundamental" law for transport in porous media (33). Nevertheless, many successes have been scored with this approach, but caution is always advised. With that proviso, we shall examine the governing laws which are of significance to our topic.

The equation for mass continuity is one of the few laws of transport in porous media that are beyond controversy, although it can be expressed in several forms. In our case, we must include a source term for vaporization or condensation. Assuming constant porosity and one-dimensional flow, the proper form for the gas phase is

$$\varepsilon\frac{\partial\rho}{\partial t}+\frac{\partial(\rho u)}{\partial x}=r_b \qquad (1)$$

where ε is the porosity, ρ is the density, u is the superficial velocity (volumetric flow rate divided by area), and r_b is the local volume-averaged rate of evaporation in kg/sm^3 [adapted from (34), p. 150].

In complex cases where the empirical Darcy's law may not suffice, an approximate form of the momentum equation can be obtained from the Navier-Stokes equations by incorporating Darcy's law and adding nonlinear extensions [adapted from (35)]:

$$\frac{\rho}{\varepsilon}\left(\frac{\partial u}{\partial t}+u\frac{\partial u}{\partial x}\right)=\frac{-\partial P}{\partial x}+\frac{1}{\varepsilon}\frac{\partial}{\partial x}\left(\mu\frac{\partial u}{\partial x}\right)-\left(\frac{\mu}{K}+\frac{\rho C|u|}{\sqrt{K}}\right)u \qquad (2)$$

Here P is the pressure, μ is the vapor viscosity, K is the permeability, and C is an empirical constant. The term containing C [Forchheimer's correction (36)] accounts for inertial effects, which are unlikely to be important at the low gas velocities involved in impulse drying. C has therefore been set to zero. Viscosity and all other gas and liquid properties are temperature dependent, with values given by regression of measured properties over the broad temperature range of interest.

The two terms in Equation 2 containing $\partial u/\partial x$ would be zero if the gas density did not change. In most cases of flow through porous media, the transient term $\partial u/\partial t$ is also small compared to other terms. These terms were included for completeness, but were recently found to be relatively unimportant in predictions of impulse drying under practical conditions. However, they give MIPPS-I the ability to handle some extreme effects in gas-phase flow. (Note that elimination of the minor terms reduces Equation 2 to Darcy's law, $u = -K/\mu^* dP/dx$.)

The energy equation for the gas phase is obtained by volume-averaging a form of the continuum energy equation [Equation. 10.1.19. of (34)], resulting in

$$(\rho C_v)_m \frac{\partial T}{\partial t} + (\rho C_v)_f u \frac{\partial T}{\partial x} = \frac{\partial}{\partial x}\left(k_e \frac{\partial T}{\partial x}\right) - P\frac{\partial u}{\partial x} + r_b h_v \ , \qquad (3)$$

where C_v is the constant-volume heat capacity, P is the vapor pressure, h_v is the heat of vaporization, and k_e is the effective thermal conductivity, defined as

$$k_e = \varepsilon k_{fluid} + (1-\varepsilon) k_{solid} \ . \qquad (4)$$

In this case, the fluid is steam and the solid is cellulose. Physical properties averaged over the entire medium or over the fluid phase alone (37) are referenced, respectively, with the subscripts m and f:

$$(\rho C_v)_m = (1-\varepsilon)(\rho C_v)_{solid} + \varepsilon(\rho C_v)_{fluid} \ , \qquad (5)$$

$$(\rho C_v)_f = \varepsilon(\rho C_v)_{fluid} \qquad (6)$$

Vaporization and condensation is assumed to occur at boundaries, so the last term in Equation 3 is not applicable to most of the flow.

The liquid phase is assumed to be incompressible, giving $\partial u/\partial x = 0$ for the continuity equation. Heat transfer in the liquid phase is given by

$$(\rho C_p)_m \frac{\partial T}{\partial t} + (\rho C_p)_f u \frac{\partial T}{\partial x} = \frac{\partial}{\partial x}\left(k_e \frac{\partial T}{\partial x}\right), \qquad (7)$$

where C_p is the constant-pressure heat capacity, and the definitions of Equations 4-6 apply, with water as the liquid phase.

The transient liquid velocity is given by the momentum transport equation modified for incompressible flow in porous media:

$$\frac{\rho}{\varepsilon}\frac{\partial u}{\partial t} = \frac{-\partial P}{\partial x} - \frac{\mu u}{K}, \qquad (8)$$

where gravitational and inertial effects have been ignored. By applying the continuity equation to convert the partial differential into an ordinary differential, a macroscopic equation for the liquid velocity can be obtained:

$$\frac{1}{\varepsilon}\frac{du}{dt} = \frac{1}{\rho}\frac{P_{int} - P_\infty}{L - x_f} - \frac{u}{K\rho}\frac{\int_{x_f}^{L} \mu(T(x))\,dx}{L - x_f}, \qquad (9)$$

where L is the thickness of the porous medium (the sheet), x_f is the location of the interface, P_{int} is the pressure at the interface, and P_∞ is the specified pressure at the exit boundary of the system.

Boundary Conditions

The metal surface in contact with the paper is the upper boundary. This boundary is given a constant temperature. Fluid velocity is also set to zero there. At the paper-felt interface, the effective thermal conductivity is set to zero. This condition allows heat to be removed by convection but implicitly assumes that water entering the felt is no longer in thermal contact with the sheet. The liquid velocity at the outlet boundary is the same as the bulk liquid velocity. The pressure at this boundary is specified and constant (typically atmospheric pressure).

The gas and liquid phases are joined through boundary conditions at the interface. The interface is a common boundary between the two phases with a single temperature, velocity, and pressure. The temperature and pressure are required to be in equilibrium. Equilibrium data for water are approximated with empirical functions (38). The rate of evaporation or boiling which occurs at the flat vapor-liquid interface is most conveniently expressed using a superficial rate, $\dot{m}_e$, having units of kg/sm^2, rather than using the local rate of boiling per unit volume, r_b in kg/sm^3. The relation between the two terms is given by

$$r_b = \dot{m}_e/\Delta x \ , \qquad (10)$$

where Δx is the thickness of the zone in which the boiling takes place (in the finite difference scheme, it is the length of the node next to the interface).

The velocity of the interface is the liquid velocity plus contributions from capillary wicking and from evaporation or condensation at the interface:

$$V_{int} = \frac{1}{\varepsilon}\left(U_L + \frac{\dot{m}_e + \dot{m}_r}{\rho_L}\right), \qquad (11)$$

where V_{int} is the interface velocity, U_L is the bulk liquid velocity, $\dot{m}_e$ is the evaporation rate (a negative number for condensation), and $\dot{m}_r$ is the capillary resupply (wicking) rate. The evaporation rate is determined by the difference between the incoming heat flux from the gas phase and the outgoing heat flux into the liquid phase:

$$\left(-k_e \frac{\partial T}{\partial x}\right)_G - \left(-k_e \frac{\partial T}{\partial x}\right)_L = \dot{m}_e h_v \,, \tag{12}$$

where the subscripts G and L refer to the gas and liquid phases, respectively.

Capillary effects cause a discontinuity in pressure at the vapor-liquid interface given by

$$P_g - P_l = \frac{2\sigma}{r_e}, \tag{13}$$

where P_g is the gas pressure, P_l is the pressure of the liquid, and σ is the surface tension, and r_e is the effective radius of curvature of the meniscus. The curved interface also affects the equilibrium condition of the vapor and liquid. The equilibrium pressure of the liquid at a given temperature can be found iteratively with the relationship (39):

$$P_o - P_l = \frac{\rho_l RT}{M} \ln \frac{P_o}{P_l + \frac{2\sigma}{r_e}} \tag{14}$$

where P_o is the saturation pressure of the liquid in a large volume (i.e., with a flat meniscus).

Capillary forces are responsible for the assumed mechanism of capillary resupply, but the resupply rate is not calculated but is an input parameter. Mass and energy balances are still satisfied as water from the saturated interface is wicked back to the surface to undergo evaporation.

Initial conditions assume an isothermal, saturated sheet with a thin zone of vapor having already developed at the upper surface of the sheet (this simplifies the start-up procedure).

Numerical Solution

The transport equations are discretized into time-implicit finite-difference equations. An iterative approach is required for each time step. The equations are solved on a moving, nonuniform, staggered grid, with a node always being kept on the advancing interface. Equilibrium between the gas pressure at the interface and the liquid temperature at the interface was also maintained iteratively. Details of the numerical solution procedure can be found in (40). In general, the methods outlined by Patankar (41) were used for much of the numerical development, including a compressible-form of the SIMPLE procedure for solving for the gas-phase pressure profile.

The resulting code has been tested for thermodynamic accuracy, physical reasonableness (given the initial assumptions), and numerical stability in several ways. It appears that the code operates as intended and does provide solutions to the physical problem described by the chosen equations.

MIPPS-I RESULTS

The cases reported here were computed using an initial liquid temperature of 100°C, a constant surface temperature of 327°C (600°K), a sheet thickness of 1.0 mm, a porosity of 0.5, and an ambient pressure of 1.013×10^5 Pa (1 atm). An effective pore radius of 5 μm was also assumed in the treatment of capillarity. Only permeability and water resupply rate were varied in the following predictions.

Interface Motion

Figure 9 shows MIPPS predictions of interface motion for two different permeabilities at a constant wicking rate of 0.5 kg/sm^2. The predictions show 60% of the free water is displaced within 50 milliseconds when the paper has a permeability of 1.0×10^{-15} m^2. Displacement is about 3 times as rapid when the permeability is increased by a factor of 10. These rates are

consistent with observed dewatering rates in impulse drying of linerboard, for which the permeability under compression should be on the order of 10^{-15} m^2 (42).

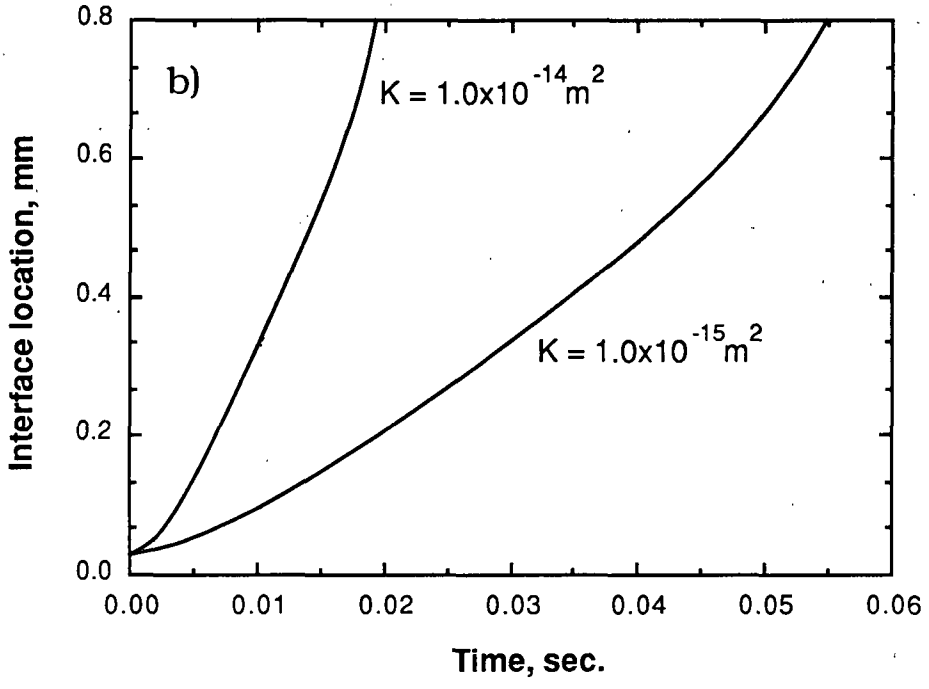

Figure 9. MIPPS-I predictions of interface motion for two different permeabilities. Data are from the same runs as those of Figure 9.

Predicted interface velocities follow a general trend: the initial velocity accelerates slowly from zero to high values near the end of the event (i.e., the second derivative of interface position with respect to time is positive). Experimental observations do show that little additional dewatering (compared to wet pressing) occurs in impulse drying unless the nip residence time exceeds some threshold value.

The predictions also show a strong dependence on wicking rate, as seen in Figure 10. A permeability of $1.0x10^{-15}$ m^2 was assumed, with wicking rates ranging from 0 to 1.0 kg/sm^2. The effect of wicking becomes more pronounced with time. Wicking

greatly increases the rate of dewatering because it increases the evaporation rate and allows higher gas-phase pressure to develop.

The model predicts the flow of vapor in the gas phase, and shows that the gas velocities are several times greater than the bulk liquid velocity as the evaporated fluid from wicking continually flows toward the cool zone where it condenses. The cyclical process of vaporization and condensation means that the total volume of vapor in the sheet at any time is much smaller than it would be if all the evaporated water had remained in the vapor phase, a simple but important fact which has been overlooked in some discussions of impulse drying.

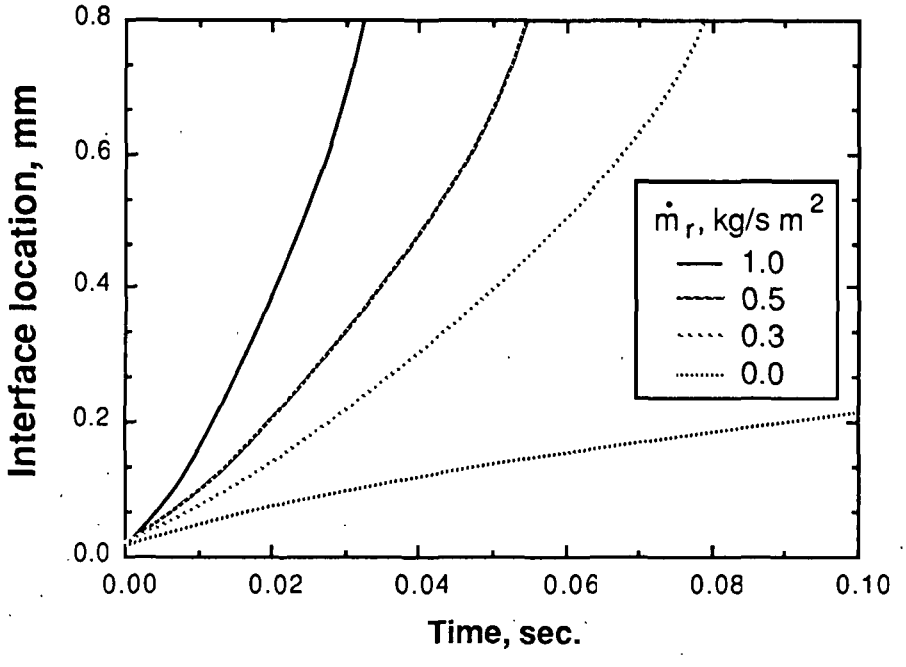

Figure 10. Predicted interface motion as a function of wicking rate in a 1-mm sheet with a permeability of 1.0×10^{-15} m^2. Head temperature is 330°C.

Vapor Pressure Development

Figure 11 presents the vapor pressure predictions for the same cases shown in Figure 9 above. An order of magnitude change in permeability changes the magnitude of the peak gas pressure by a factor of about 3, a result seen in many other MIPPS-I predictions. The range of predicted pressures encompasses the peak vapor pressure of 0.6 MPa gauge reported by Burton (2), and the shapes of the profiles correspond with his reported curve up to the point where the mechanical pressure was relieved. There are uncertainties in his experimental method, however, and accurate measurement of internal vapor pressure may still be an elusive goal. The temperature propagation data of Sprague (5) can be used to infer vapor pressures during some portions of the drying event by noting the temperature of the two-phase zone, if one can be distinguished. The temperature data suggest a broad range of vapor pressures, roughly 0.05 to 0.3 Mpa. The permeability and porosity of the lightweight sheets are not known. (Note that the higher vapor pressures in Figure 11 are partly due to the high assumed thickness of the sheet; a thinner sheet provides more pressure relief. A thick 1-mm sheet was used as a base for much of the modeling work.)

Examination of Figures 9 and 11 shows that when the permeability is lower, the increasing vapor pressure gets less relief from the moving liquid seal and thus higher pressures are achieved. The higher pressure means a greater force for liquid removal, which partly compensates for the increased resistance to flow. This is one factor which may contribute to the small pressure-dependency seen in the data for extra water removal presented above.

As mentioned above, the presence of a pressurized vapor zone penetrating into the sheet may mean that significant gains in sheet dryness are possible through reducing rewet as well as by direct displacement.

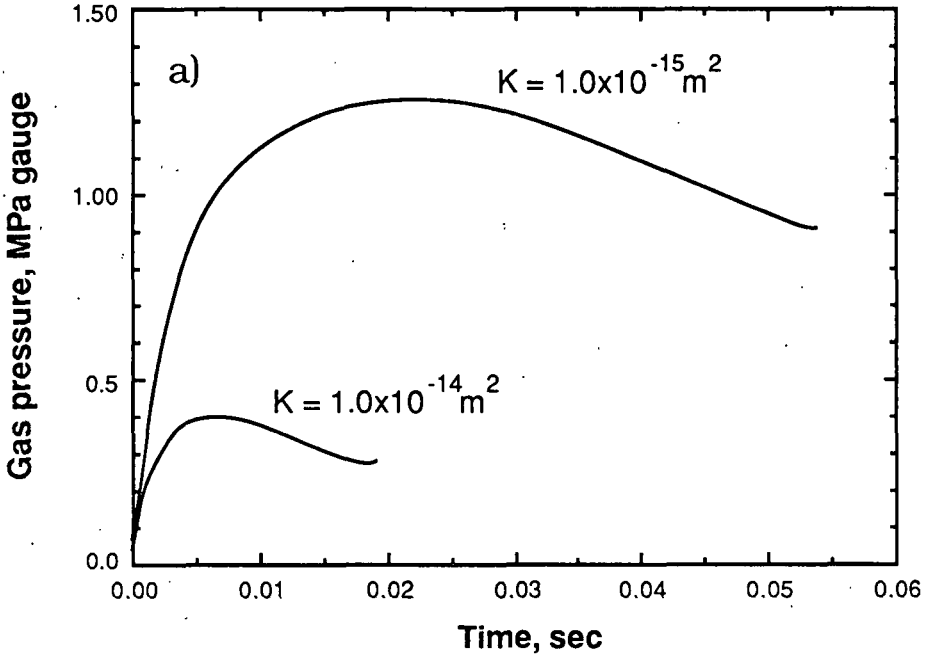

Figure 11. MIPPS-I predictions of vapor pressure development in a 1-mm sheet for two different permeabilities. Data are from the same computer runs shown in Figure 9.

Heat Flux

MIPPS predictions of the transient heat flux rate show that significant wicking is required (given the assumptions of MIPPS-I) to explain the observed heat fluxes. Conduction alone between a hot metal surface and a cool saturated sheet can account for the peak which occurs at the beginning of the process, but without a continued boiling process near the surface, the observed heat transfer rates after the tail are underpredicted by a factor of roughly 2 or more. While MIPPS-I predicts that a boiling process can occur without capillary resupply (a natural result of the thermodynamics), the predicted rate of boiling is too low unless a supply of liquid is brought near the hot surface in spite of the growing vapor zone.

Figure 12 compares MIPPS predictions with experimental heat flux data from Lavery (4). Lavery used a 125 g/m^2 virgin kraft linerboard sheet at 35% solids and 75°C with a hot surface temperature of 315°C. The physical properties of the linerboard are not known accurately, although a permeability of roughly 10^{-15} m^2 for the compressed linerboard should be reasonable. As mentioned in the previous discussion of model assumptions, the predictions begin in the portion of the pressing event in which little compression of the paper occurs (i.e., where the assumption of a rigid porous medium is appropriate). Again, comparisons of impulse drying data with MIPPS predictions must be viewed cautiously because MIPPS does not simulate the full impulse drying event.

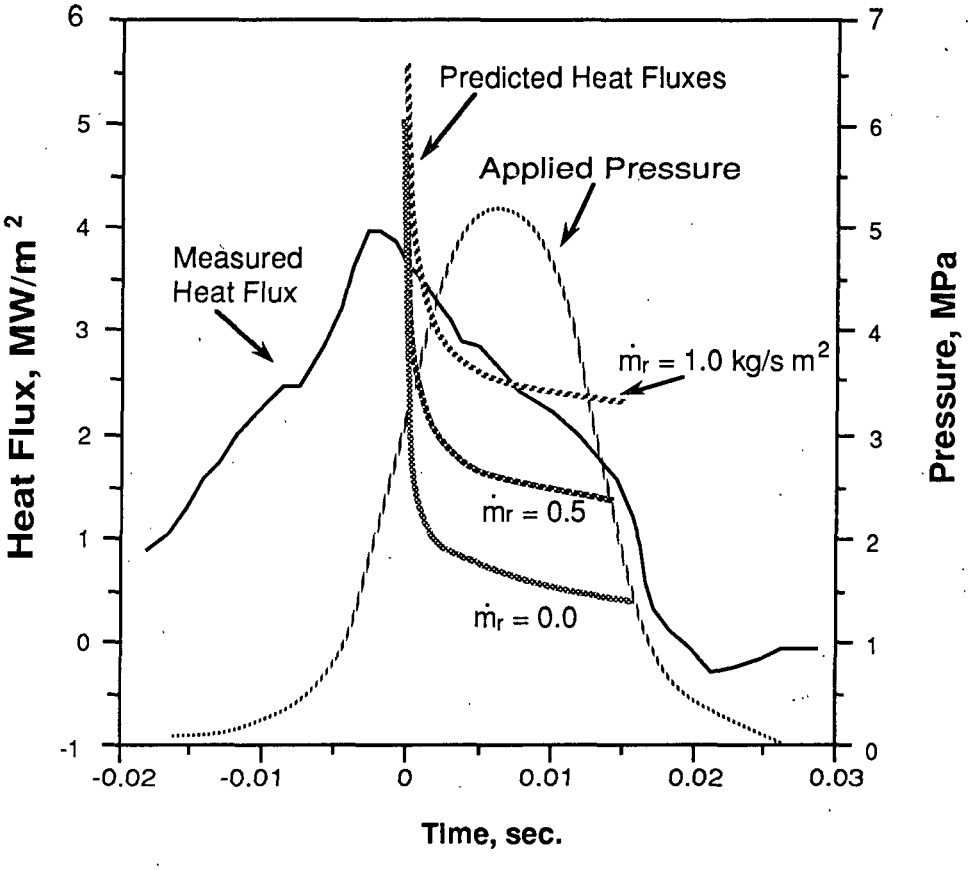

Figure 12. Comparison of MIPPS-I predictions with heat flux data from Lavery (4). Three capillary wicking rates are used in the prediction. Predictions used a head temperature of 330°C.

Three values of wicking rate were used in the predictions of Figure 12, one of which (1.0 kg/sm^2) corresponds with a portion of the experimental data. (The same prediction is actually more similar to Burton's heat flux measurement of linerboard under similar conditions, presented in Figure 3 above, but pressure pulse information was not reported.) Constant wicking rates were used in the predictions, while in reality the wicking rate will decrease as the interface moves away from the heated surface. MIPPS predictions made with a decreasing wicking rate give improved agreement, but because of the *ad hoc* nature of the wicking rate, improvements should be sought by more rigorously treating the possible two-phase wicking zone rather than empirically adjusting a wicking function.

Alternate explanations for the high experimental heat flux rates have been explored. One possibility is that water contained in the lumens of fibers near the surface is insulated, and only slowly becomes hot enough to boil. The vaporization of chemically bound water may also be delayed. These hypotheses were tested by measuring heat fluxes in the impulse drying of wet fiberglass sheets (43). The glass fibers were also examined with an electron microscope, showing them to be solid cylindrical rods.

A sample heat flux result is given in Figure 13. While the permeability and pore structure of fiberglass differ from paper, the measured heat flux curves show similar trends. While high initial peaks were not always observed, there were high sustained heat fluxes that require more than conduction to explain. The heat fluxes require capillary wicking rates on the order of 0.2 kg/sm^2 to be consistent with MIPPS-I predictions. The lower wicking rate in fiberglass matt compared to paper correlates with the more open pore structure of fiberglass (larger pore sizes, with fewer small pores available for wicking).

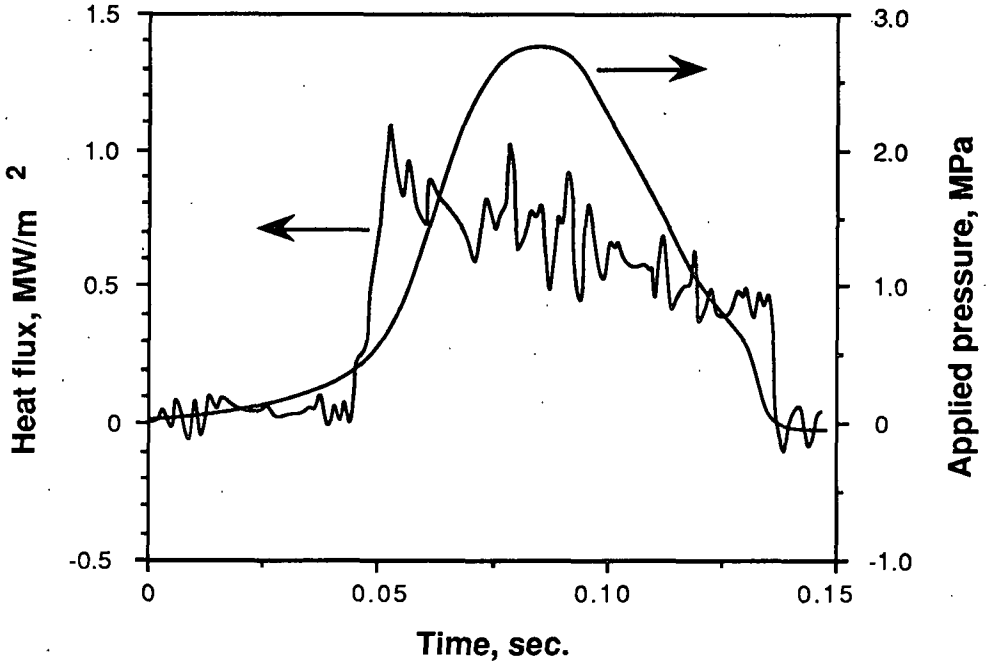

Figure 13. Typical heat flux measurement during the impulse drying of a wet fiberglass sheet (commercial insulation). Head temperature was 240°C.

In general, for the impulse drying of paper, it appears that wicking rates on the order of 0.5 kg/sm^2 in paper are needed in MIPPS-I to match the measured rates of heat transfer. Such wicking rates also lead to interface motion consistent with the observed water removal rates in impulse drying. By no means does this prove that capillary flow is important or even occurs; but it does show how a heat pipe mechanism may be consistent with observations. Note that the capillary flow rates implied by MIPPS-I are physically reasonable. The predicted pressure drop in the vapor region is always small enough to permit rapid capillary wicking in the smaller pores. For instance, if water is wicked to the surface across a 200 μm thick zone through pores 1 μm in diameter, less than 1% of the surface area of the sheet must be occupied by such pores to provide 1.0 kg/sm^2 of water to the surface, given a negligible gas-phase pressure gradient.

Temperature Histories

In Figure 14, MIPPS-I predictions of temperature propagation are shown for several locations within a sheet. A capillary resupply rate of 0.1 kg/sm^2 was used. Some relation to the experimental data of Figures 7 and 8 is evident, although there is no isothermal two-phase zone. However, the predicted concave-up temperature rise due to conduction into a liquid zone is evident in the data, as well as the rapid concave-down temperature rise which is predicted once a dry zone has passed over the measurement point. Because the predictions used an assumed initial sheet temperature of 100°C while the experimental work of Sprague (5) used room-temperature sheets, the initial warm-up zone is less pronounced in the predictions.

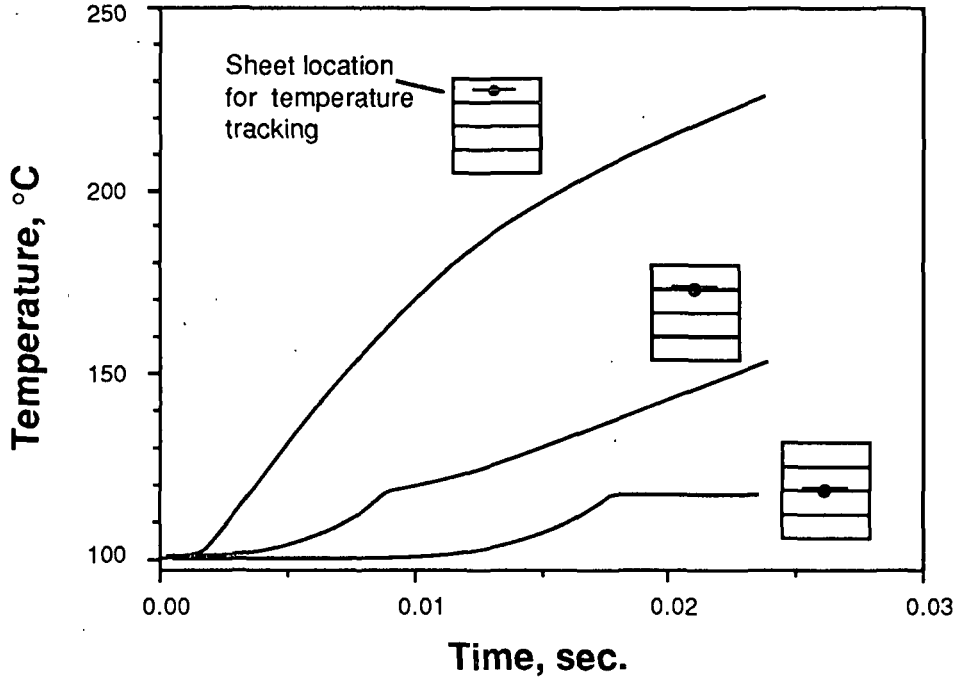

Figure 14. MIPPS-I predictions of local temperature histories at 3 locations in a 1-mm sheet. Surface temperature was 330°C, wicking rate was 0.1 kg/sm^2.

The plateau region in the bottom curve of Figure 14 late in the impulse drying process is not due to a two-phase zone region, but occurs because the pressure in the vapor region is dropping as the vapor zone nears the felt, and the corresponding equilibrium processes result in a fairly stable temperature at the middle of the sheet. If the flat region were then followed by a steep rise in temperature, then a two-phase zone followed by a dry-zone would be implied (an isothermal two-phase zone, of course, is not possible in MIPPS-I).

Figure 15 shows a prediction similar to that of Figure 14 except that the capillary resupply mechanism has been turned off. Several minor features in the curve shapes differ, and the time required for temperature rise is much greater. Both predictions, however, show qualitative features found in some of the experimental results (see Figures 7 and 8), with the notable exception that two-phase zone effects can be deduced in many of the observed profiles. It was this exception which first suggested that MIPPS needed to be improved by permitting a two-phase zone to develop.

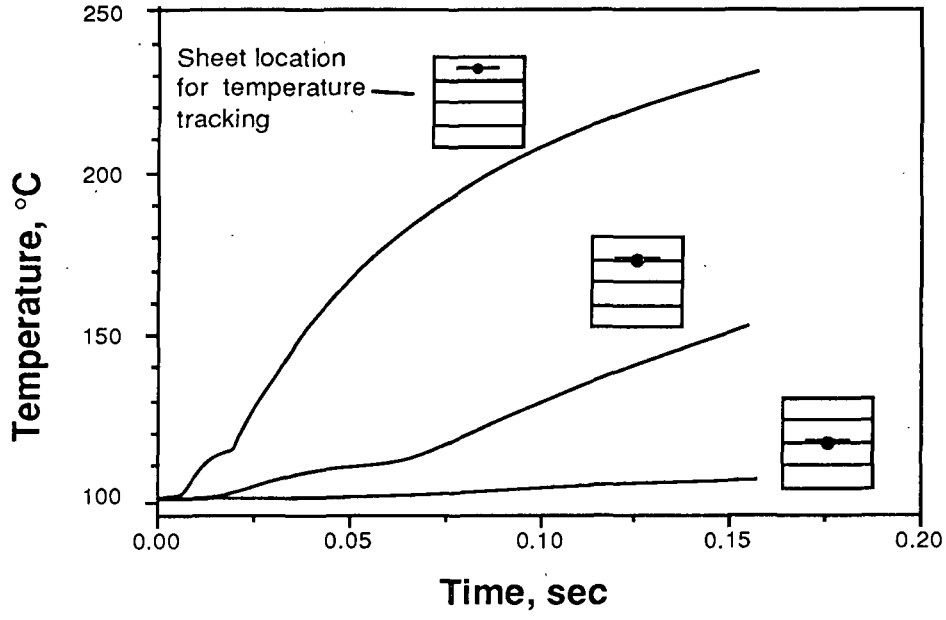

Figure 15. MIPPS-I predictions of local temperature histories at 3 locations in a sheet. Conditions are the same as those in Figure 14, but the capillary wicking rate is zero.

MIPPS-II: A DIFFERENT APPROACH

The Need to Account for a Two-Phase Zone

While the sharp-interface of MIPPS-I appeared to be consistent with some data, the temperature propagation data above show that it is incorrect. Since a sharp interface can be a special case of a two-phase zone, a model permitting a two-phase zone to develop could be more general. Furthermore, the troublesome *ad hoc* correction of a wicking rate might be avoided in favor of a more realistic system by handling computations with a two-phase zone. On the other hand, the complexities of transient flow and heat transfer in a two-phase zone can be formidable, and rigorous modeling would require experimental parameters and properties that are simply unavailable for paper. Then again, it might be possible to lump many of the unknowns into one or two parameters that have a fundamental relation to intrinsic paper properties. The decision was thus made to develop a new model to examine some aspects of impulse drying with a two-phase zone.

In considering a two-phase zone, it became clear that some of the heat transfer ascribed to capillary wicking above may be due to liquid trapped in or around fibers after all. While heat flux results with fiberglass sheets were initially interpreted as evidence for capillary resupply as opposed to the boiling of trapped liquid, one factor was overlooked until recently. The glass fibers do not have lumens, but there is the possibility that water is trapped in dead-end pores between the fibers as the vapor front moves, and that the trapped or residual water gives rise to a two-phase zone which can supply liquid for boiling near the surface.

Apparently any fibrous porous medium can have a significant fraction of the pore volume occupied by dead end pores (44), and if these pores remain filled with fluid after the vapor phase has passed by, a source of liquid for boiling will be available. This possibility is considered in detail below.

Model Development: New Simplifications

Adding two-phase capabilities required a fundamental rewriting of the code. In investigating the performance of MIPPS-I, it became clear that further simplifications in the transport equations were possible without sacrificing pre-

dictive power. For instance, direct evaluation of all non-Darcian terms in the momentum equation (Equation 2) during runs with MIPPS-I showed that these terms were negligible. Furthermore, since the predicted pressure drop in the gas phase was always much less than the pressure drop across the liquid zone, there was no significant need to solve for the gas pressure distribution except in cases with high resupply rates where gas velocity becomes appreciable. If one assumes that the gas pressure changes in time but is spatially uniform, the solution procedure becomes much simpler. In fact, the more tractable solution procedure allows saturation gradients and other factors to be considered that would have been difficult to treat otherwise.

The Two-Phase Zone

The modeling of saturation gradients during two-phase flow is far from trivial. As a gas displaces a liquid, there may not be a sharp interface but a zone of changing saturation. This arises from both capillary forces and the effects of relative permeabilities. Models of this sort rely on equilibrium saturation curves to relate moisture content and capillary pressure. A key parameter from these measurements is the irreducible liquid saturation, or the amount of liquid left behind in a porous matt which no amount of capillary pressure can remove. The irreducible saturation, however, is obtained near equilibrium in a measurement process that can last several days or even weeks, whereas the amount of fluid left behind in a rapid vapor-liquid displacement process can be much greater. The amount of remaining fluid in nonisothermal, transient displacement may be much different, but should be a measure of the trapped pore volume, consisting of pores which have narrow constrictions limiting the flow of water through them, pores which have dead-end regions, and pores which are completely isolated from other pores (45).

In the absence of adequate experimental data, it was assumed that the remaining moisture fraction left behind a rapid displacement front is constant. Because the remaining water is assumed to be trapped once it is left behind, at least for the time scale of the displacement process, it has a relative permeability of zero and will remain in place until it has evaporated. If the saturated liquid zone moves away faster than the beginning of the two-phase zone is evaporated, the

two-phase zone will grow in time. Likewise a high heat flux can cause the zone to shrink.

While this approach does not require a specified resupply rate in impulse drying, it does introduce another parameter, the remaining saturation level, S_r. This factor, however, is more closely related to the inherent physical nature of the sheet than is a resupply rate. For a given sheet, S_r is expected to be a function of compression and temperature, but a constant is used as a mask for ignorance. Based on general information about wet pressing and flow in fibrous porous media, it appears that S_r could be on the order of 0.1 to 0.4, but this is largely a guess at this point.

The steam and liquid water in the two-phase zone are at equilibrium. Since the pressure drop in the gas phase is assumed to be negligible, the equilibrium conditions require the two-phase zone to be at constant temperature. Capillarity changes the equilibrium temperature for a given pressure according to Equation 14. The relation between saturation and capillary pressure will be neglected; a single value of effective meniscus curvature is used regardless of saturation.

Momentum Transfer

Flow in the gas phase is neglected, and the liquid velocity is given simply by the integral form of Darcy's law at every time step:

$$U_L = \frac{P_{int} - P_\infty}{K(L-x_f) \int_{x_f}^{L} \mu(T(x))\ dx} \quad . \tag{15}$$

Inertial forces have been neglected here.

Heat Transfer

A form of Equation 7 can be applied to the vapor and liquid zones. By neglecting flow in the gas phase, the convective term is eliminated, resulting in

$$(\rho C_p)_m \frac{\partial T}{\partial t} = \frac{\partial}{\partial x}\left(k_e \frac{\partial T}{\partial x}\right) + r_b h_v \ , \qquad (16)$$

Because the two-phase zone has constant temperature, heat transfer is governed solely by evaporation and condensation, which must occur in such a way to keep the two-phase zone temperature, T_{2P}, in equilibrium with the vapor pressure (discussed below).

Vapor Pressure Development and Vapor-Liquid Equilibrium

By neglecting the viscosity of the gas, the gas pressure in the gas phase can be assumed constant. The total mass of vapor present in the paper can be expressed in terms of either a time integral of the net evaporation rate or an integral of the local density determined with the ideal gas law:

$$w_g = \frac{PM}{R} \int_0^{x_f} \frac{\varepsilon A (1-S)}{T} \, dx = \int_0^t A \dot{m}_e \, dt'$$

$$= \int_0^t \int_0^{x_f(t)} A r_b \, dx \, dt', \qquad (17)$$

where w_g is the total mass of vapor, M is the vapor molecular weight, A is the paper surface area, and t' is a dummy variable for the time integration. The local boiling rate, r_b, is negative where condensation occurs. From Equation 17, we can obtain an expression which determines the pressure at any time:

$$P = \frac{R}{M} \frac{\displaystyle\int_0^t \int_0^{x_f(t)} A r_b \, dx \, dt'}{\displaystyle\int_0^{x_f} \frac{\varepsilon A (1-S)}{T} \, dx} \ . \qquad (18)$$

The thermodynamics of the two-phase zone require special attention. The numerical model must allow condensation and evaporation to occur throughout the zone in a way that conserves mass and energy and maintains equilibrium between temperature and pressure. Because the treatment is somewhat involved, the details are presented in Appendix A.

Boundary Conditions

Boundary conditions are similar to those of MIPPS-I, with the added complication that phase change can occur at the beginning and the end of the two-phase zone due to differences in thermal conduction (Equation 12), and phase change can occur throughout the entire two-phase zone to maintain equilibrium, as discussed in Appendix A. The initial condition assumes that a thin dry layer and a thin partially-saturated layer exist at the top of the sheet (all initial conditions are specified by an input data file for each run, and are not built into the code).

Numerical Solution

The key equations for MIPPS-II were discretized into explicit finite-difference forms using a moving, staggered grid with uniform grid spacing within a given zone. The resulting numerical procedure was substantially different from that employed in MIPPS-I; the only common elements in the two codes were the subroutines for physical property evaluation and interpolation.

Use of an explicit method simplified the code compared to the implicit solution method of MIPPS-I. While implicit methods are generally more stable than explicit methods and can therefore use larger time steps in the solution, the time-step in MIPPS-I was not limited by numerical stability but by the requirement that the interface advance no more than one cell per time step. Use of an explicit method was therefore expected to be advantageous in MIPPS-II.

MIPPS-II RESULTS

Predicted temperature histories at three sheet locations are shown in Figure 16. Some of the same features seen in the experimental measurements are evident: an S-shaped transition

from the initial temperature to a flat two-phase zone, which may be followed by a dry stage characterized by a rising, concave-down curve. The close resemblance between the features seen in the data helps validate the treatment of the two-phase zone in MIPPS-II. The data do not always show a clear two-phase zone in the upper regions of the sheet, however, suggesting that some time may be required for a sharp interface to spread into a two-phase zone.

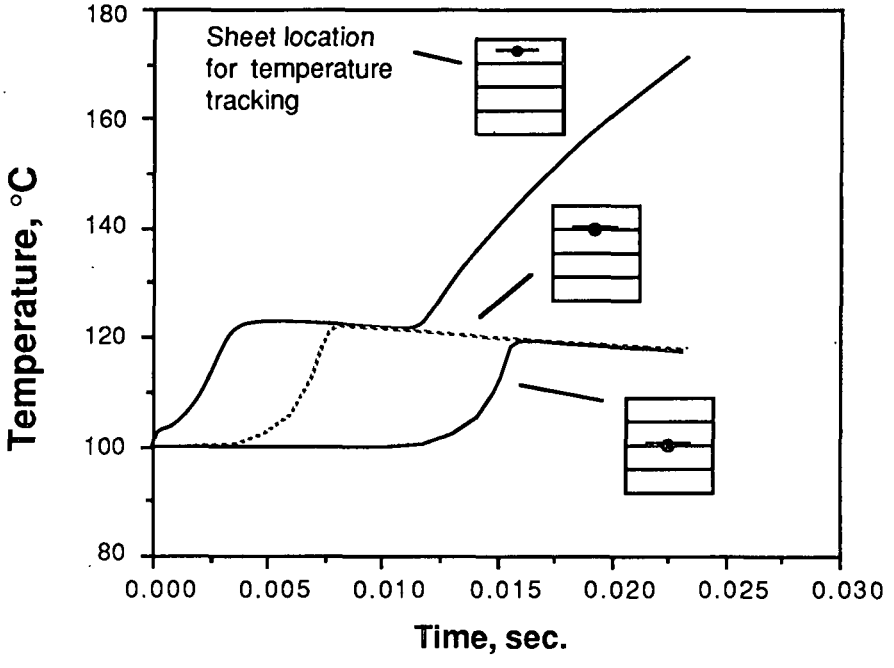

Figure 16. MIPPS-II predictions of local temperature histories in a 0.5 mm sheet with a permeability of 1.0×10^{-14} m^2. Temperatures are tracked at locations corresponding to 1/8, 1/4, and 1/2 of the sheet thickness.

One interesting feature is the similarity between MIPPS-II predictions of interface motion and pressure development with similar predictions in MIPPS-I. Figures 17 and 18 compare MIPPS-II and MIPPS-I predictions of vapor pressure development and interface location, respectively, in a sheet of permeability 1.0×10^{-14} m^2. Both predictions employed mild impulse drying conditions: the MIPPS-II predictions used a remaining water saturation of 0.1, and the MIPPS-I predictions

used a wicking rate of 0.1 kg/sm^2. That the two predictions could be so similar is noteworthy (these were the first two predictions to be compared, no trial-and-error was involved). This agreement suggests that the effect of residual water left in a two-phase zone is similar to the effect of water transported via insulated capillaries into a dry zone, and raises the possibility that either or both concepts have value.

Examination of boiling and condensation rates throughout the sheet during MIPPS-II predictions again show a continued process of boiling and evaporation. The rates of condensation are always close to the boiling rates near the hot surface. This phase change process gives high heat fluxes, beyond that of conduction alone, which correlate with experimental results. A typical heat flux curve from MIPPS-II is given in Figure 19.

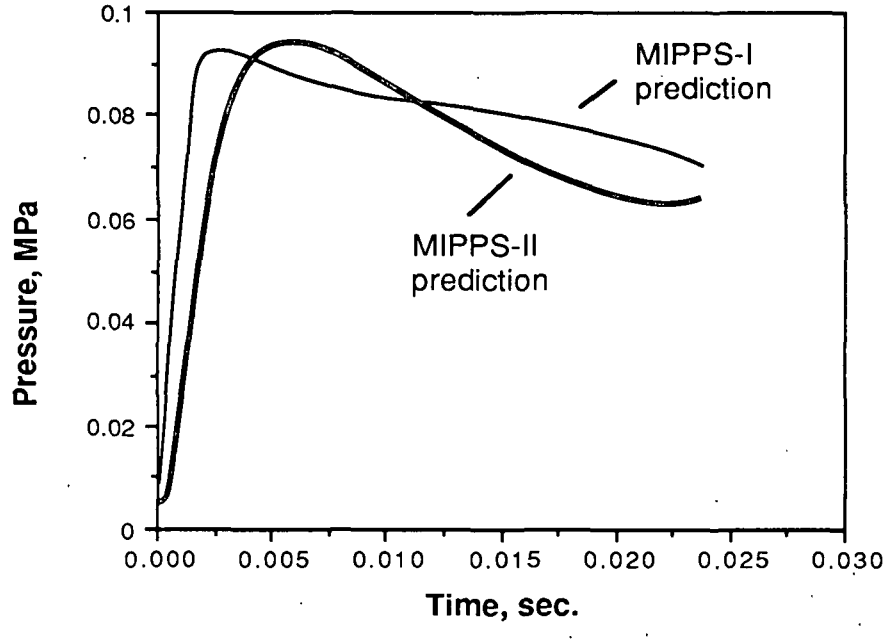

Figure 17. Predicted vapor pressure development in MIPPS-I and MIPPS-II. Sheet thickness was 0.5 mm, surface temperature 330°C, and permeability 1.0x10^{-14} m^2. MIPPS-I used a wicking rate of 0.1 kg/sm^2, and MIPPS-II used a remaining saturation value of 0.1.

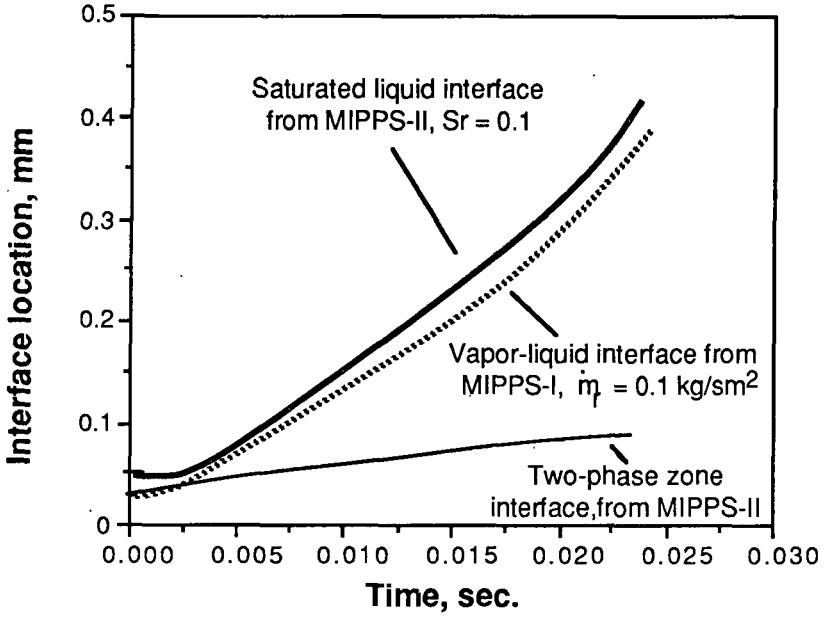

Figure 18. Interface motion predicted by MIPPS-I and MIPPS-II. Data are from the same computer runs used in Figure 17. MIPPS-II interface motion for the two-phase region is also shown.

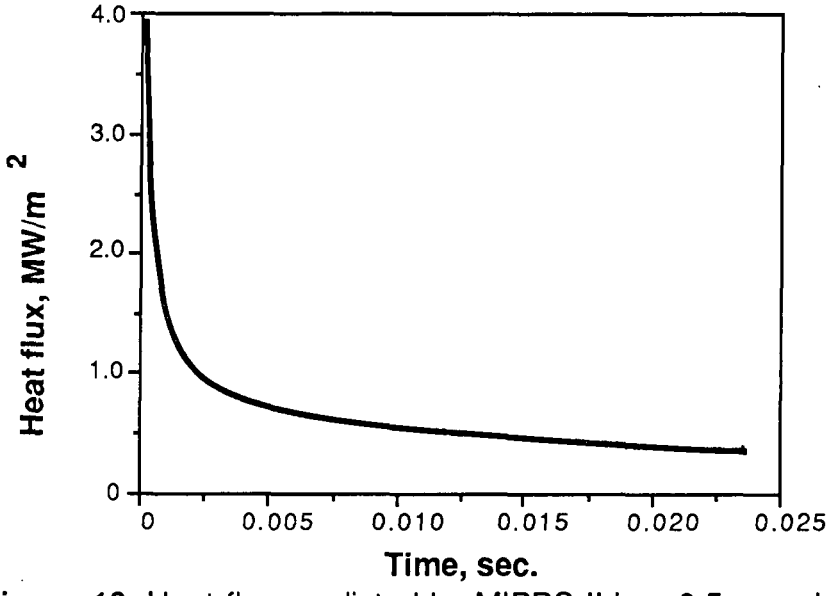

Figure 19. Heat flux predicted by MIPPS-II in a 0.5-mm sheet with permeability 1.0×10^{-14} m^2 and S_r of 0.1.

The predictions of MIPPS-II, being of a more fundamental nature than those of MIPPS-I, are sensitive to the assumed initial saturation distribution. The above predictions have been made using an initial dry zone extending 6% into the sheet. If the size of the initial dry zone (from the start-up initial condition) is reduced by a factor of 5, interface velocity can be roughly doubled. While this shows that MIPPS-II predictions must be viewed with caution (although trends and qualitative relationships do not change with initial conditions), it also suggests that the surface properties of a sheet of paper may be important in the impulse drying process. Random changes in surface porosity and saturation (due to air entrapment or other factors) may account for some of the scatter observed in impulse drying events. The importance of the heat transfer processes at the metal-paper boundary must be stressed, however, and future work should explore the possibility of treatments to the paper surface or even to the metal surface to favorably control or modify the heat transfer processes in impulse drying. Related work is underway (9).

MIPPS-II still has several serious limitations which will be addressed in the future. Compressibility of the porous medium is the most important feature which must be added. Treatment of capillary flow in the two-phase zone is also important. Furthermore, MIPPS-II has neglected the temperature gradients which may develop in the two-phase zone since regions of low saturation will have a higher equilibrium temperature than the more saturated zones.

CONCLUSIONS AND SUMMARY

Both models predict similar trends in impulse drying, but MIPPS-II offers the advantage of treating a two-phase zone which appears to exist in impulse drying. The predicted temperatures, pressures, and displacement velocities give some insights into the impulse drying mechanism, and confirm the importance of the vapor zone created by rapid phase-change heat transfer processes.

A continued process of evaporation and condensation is implied or predicted by both models. In MIPPS-I, an *ad hoc* capillary resupply term must be added to account for the observed heat transfer rates. In MIPPS-II, where the limitation of a sharp interface is removed, predictions show a continued

process of boiling at the beginning of the two-phase zone with condensation near the saturated region. The two-phase zone is heated by condensation during the early part of the impulse drying process, but when the vapor pressure begins to drop, the two-phase zone releases energy through evaporation (thus cooling the two-phase zone). This energy release (especially in the form of flashing as the sheet leaves the nip) is believed to be related to the problem of delamination. Delamination will be affected not only by the vapor pressure, but by the location of the saturated liquid interface.

The results also show that conduction can account for the high observed heat transfer rates only during the first few milliseconds of impulse drying while the cellulose is still cool and the saturated zone is near the hot surface. Once a steam layer is formed, heat transfer into the sheet gives heat transfer rates far below those observed unless a supply of liquid is made available near the surface for continued boiling. The effects of capillary flow and dead-end pores may both be important; further research is needed to understand the boiling processes in the zone next to the surface. One doctoral research project is currently focusing on this issue (46). MIPPS-II lumps the effects of capillary resupply and dead-end pores into a single residual saturation constant. Future modeling work will provide a more rigorous treatment of the separate effects. Experimental work is also needed to examine the actual residual saturation that occurs in paper or model fibrous media under dynamic impulse-drying conditions.

Sheet permeability has a strong affect on the impulse drying process. A decrease by a factor of 10 lowers the water removal rate by roughly a factor of 3 to 4 in most cases, with vapor pressure increasing by roughly a factor of 3 for the conditions examined in this study. The most rapid water removal, of course, will occur in the sheets with the lowest flow resistance; such sheets should also be free of delamination because of the lower vapor pressures involved.

The possible role of rewet reduction, as implied by the predicted high vapor pressures which persist during impulse drying, should be considered in future studies and in the interpretation of past data. The mechanism of rewet reduction will be strongly affected by basis weight and felt properties. It may lead to enhanced water removal even under conditions where only insignificant water removal by pure displacement is

possible. In any case, it does appear that the creation of a vapor zone is the key to impulse drying.

Overall, MIPPS-I and II provide limited tools with which some aspects of impulse drying physics can be explored. These numerical tools serve to complement rather than replace experimental investigations.

APPENDIX A:

THERMODYNAMICS OF THE TWO-PHASE ZONE IN MIPPS-II

The thermodynamics of the two-phase zone need special attention. At each time step, the pressure has changed because of phase change and also because of expansion or contraction due to temperature changes. The liquid in the two-phase zone must remain in equilibrium with the vapor. This is achieved in a manner which conserves energy and mass. If the temperature of the two-phase zone is not in equilibrium with the current pressure, condensation of the gas phase or evaporation of the liquid phase is assumed to take place instantaneously (at least within one time step) and uniformly over the two-phase zone in order to bring the pressure and temperature into equilibrium. For instance, if the current temperature is lower than the equilibrium temperature for the newly computed gas pressure, some of the gas phase condenses, lowering the gas pressure and at the same time raising the temperature of the two-phase zone due to the released latent heat of vaporization. The mass and enthalpy of the system are conserved in this process.

When condensation occurs, some of the vapor previously outside the two-phase zone will move in in order to maintain uniform pressure. Let Δm be the superficial mass (mass per unit area of paper) of condensate necessary to bring the temperature into equilibrium with the resulting pressure. The mass which enters the two-phase zone from the dry zone is given by $(1-f_g)\Delta m$, where f_g is the mass fraction of the total vapor contained in the two-phase zone. It can be obtained by considering the ideal gas law and the amount of volume available to the gas:

$$f_g = \frac{\int_{x_d}^{x_f} \frac{\varepsilon(1-S)\ dx}{T}}{\int_{0}^{x_f} \frac{\varepsilon(1-S)}{T}\ dx} \tag{A1}$$

An enthalpy balance gives the new two-phase zone temperature after condensation, T_{2P}^{*}, as:

$$T_{2P}^{*} = T_{2P}^{0} + \frac{\Delta m\ h_v(T_{2P}^{0})}{(m_g - f_g\Delta m)\,C_{pg} + (m_l+\Delta m)\,C_{pl} + m_s C_{ps}}$$

$$\equiv T_{2P}^{0} + \frac{\Delta m}{\gamma} \tag{A2}$$

where T_{2P}^{0} is the temperature before condensation, and m_g, m_l, and m_s are the superficial masses of gas, liquid, and solid, respectively, in the two-phase zone. The parameter γ is a ratio of thermal mass to heat of vaporization, and is only a weak function of Δm when the mass of the condensate is small compared to the mass in the two-phase zone. All physical properties in Equation A2 are evaluated at the known temperature, T_{2P}^{0}.

Now the loss of the condensate from the gas phase leads to a change in pressure, ΔP. The relationship is given by:

$$\Delta m = -\Delta P \frac{MW}{R} \int_{0}^{x_f} \frac{\varepsilon(1-S)}{T}\ dx \equiv -\beta\Delta P \tag{A3}$$

where ΔP is the difference between the pressure before and after condensation. The resulting pressure, P^{*}, is given by

$$P^* = P^0 + \Delta P = P^0 + \frac{\Delta m}{\beta} \quad . \tag{A4}$$

The goal is to choose Δm such that P^* and T^*_{2P} are in equilibrium. The temperature in equilibrium with a given pressure is expressed by the function $T_{eq}(P)$. If ΔP is small, then a linear approximation is possible:

$$T_{eq}(P^0+\Delta P) \cong T_{eq}(P^0) + \alpha\Delta P \quad , \tag{A5}$$

The equilibrium condition is

$$T_{eq}(P^0+\Delta P) = T^*_{2P} \tag{A6}$$

which forces Δm to be

$$\Delta m = \frac{T_{eq}(P^0) - T^0}{\left(\frac{1}{\gamma} + \frac{\alpha}{\beta}\right)} \quad . \tag{A7}$$

Once Δm has been determined, the new equilibrium pressure and temperature is given by Equations A4 and A5. The determination of Δm must be iterative, however, because γ is a function of Δm. By iteratively adjusting α in Equation A5 as well, the linear approximation can be made exact for the known interval, ΔP. Usually three or four iterations suffice to obtain a stationary value of Δm.

This equilibrating phase-change process changes the saturation in the two-phase zone. The amount of the total condensate, Δm, distributed to each cell is determined by a form of Equation A7 written for individual cells such that the temperature of each cell is brought to the new zonal equilibrium value. The amount of condensate needed per cell is not uniform because saturation and hence thermal properties may vary from cell to cell.

REFERENCES

1. Lavery, H., Project 3470 Status Report to the Engineering Project Advisory Committee, The Institute of Paper Chemistry, Appleton, Wisconsin (Oct. 22, 1987).

2. Burton, S. W., "An Investigation of Z-direction Density Profile Development During Impulse Drying," Ph.D. Thesis, The Institute of Paper Chemistry, Appleton, Wisconsin (1986).

3. Burton, S. W., and Sprague, C. H., "The Instantaneous Measurement of Density Profile Development During Web Consolidation," J. Pulp Paper Science, 13 (5): J145 (1987).

4. Lavery, H. P., "New Mechanisms for Water Removal From Paper Through Impulse Drying," AIChE Summer Meeting, Minneapolis, Minnesota (Aug. 16-20, 1987). Also printed as IPC Technical Paper Series #251, The Institute of Paper Chemistry, Appleton, Wisconsin (July, 1987).

5. Sprague, C. H., to be presented at the Ninth Fundamental Research Symposium, Cambridge, England (Sept. 16-22, 1989).

6. Winter, E. R. F. and Barsch, W. O., "The Heat Pipe," Advances in Heat Transfer, ed. by T. F. Irvine and J. P. Hartnett, Vol. 7, New York: Academic Press (1971).

7. Dreshfield, A. C., "The Drying of Paper," Tappi, 39 (7): 449 (1956).

8. O'Neill, B. M., "Blade Coating as a Means of Producing Paper Grades of High Performance," Appita J., 31 (2): 135-141 (1977).

9. Santkuyl, R., M.Sc. Project, The Institute of Paper Chemistry, Appleton, Wisconsin, (in progress, 1989).

10. Zavaglia, J., and Lindsay, J. D., "Flash X-ray Visualization of Multiphase Flow in Impulse Drying," to be presented

at the 1989 Tappi Engineering Conference, Atlanta, Georgia (Sept. 1989).

11. Kloth, G., Sprague, C. H., and Hartman, T., "Water Movement in the Web of a Rolling Wet Press Nip Viewed with Flash X-ray Radiography," to be presented at the 1989 Tappi Engineering Conference, Atlanta, Georgia (Sept. 1989).

12. Macklem, E. A., and Pulkowski, J. H., "Impulse Drying-A Pressing/Flashing Drying Phenomena," 1988 Tappi Engineering Conference, Chicago, Illinois (Sept, 19-22, 1988).

13. Rogers, J., "A Study of Rewetting in Impulse Drying Using Flash X-ray Radiography," M.Sc. Thesis, The Institute of Paper Chemistry, Appleton, Wisconsin (in progress, 1989).

14. Pounder, J. R., "A Mathematical Model of High Intensity Paper Drying," Ph.D. Thesis, The Institute of Paper Chemistry, Appleton, Wisconsin (January, 1986).

15. Ahrens, F., "Wet Pressing Fundamentals," Project 3480 Status Report, The Institute of Paper Chemistry, Appleton, Wisconsin (Sept. 1984).

16. Hartley, F. T., and Richards, R. J., "Hot Surface Drying of Paper— The Development of a Diffusion Model," Tappi, 57 (3): 157 (1974).

17. Lee, P. F., and Hinds, J. A., "Analysis of Heat and Mass Transfer Within a Sheet of Papermaking Fibers During Drying," Drying '82, ed. Mujumdar, A. S., Washington, D. C.: Hemisphere Publishing Corporation (1982).

18. Ahrens, F., and Journeaux, I., "An Experimental and Analytical Investigation of Thermally Induced Vacuum Drying Process for Permeable Mats," Drying 84, ed. Mujumdar, A. S., Washington, D. C.: Hemisphere Publishing Corp. (1984).

19. Milly, P. C. D., "Advances in Modeling of Water in the Unsaturated Zone," Transport in Porous Media, 3 (5): 491 (1988).

20. Pollock, D. W., "Simulation of Fluid Flow and Energy Transport Processes Associated with High-level Radioactive Waste Disposal in Unsaturated Alluvium," Water Resources Research, 22: 765-775 (1986).

21. Gottardi, G. and Mesini, E., "A Two-phase Finite-Element Program for Displacement Simulation Processes in Porous Media," Computers and Geosciences, 12 (5): 667 (1986).

22. Homsy, G. M., "Viscous Fingering in Porous Media," Ann. Rev. Fluid Mechanics, 19: 271 (1987).

23. Gorell , S. B. and Homsy, G. M., "A Theory for the Most Stable Variable Viscosity Profile in Graded Mobility Displacement Processes," AIChE J. 31 (9): 1498 (1985).

24. Udell, K. S., and Fitch, J. S., "Heat and Mass Transfer in Capillary Porous Media Considering Evaporation, Condensation and Non-Condensible Gas Effects," Heat Transfer in Porous Media and Particulate Flows, Proceedings of the 23rd National Heat Transfer Conf., Denver, Colorado (Aug. 4-7, 1985).

25. Crank, J., "How to Deal with Moving Boundaries in Thermal Problems," Numerical Methods in Heat Transfer, ed. Lewis, R. W., Morgan, K., and Zienkiewicz, O. C, New York: John Wiley and Sons (1981).

26. Ockendon, J. R., and Hodgkins, W. R., editors, "Moving Boundary Problems in Heat Flow and Diffusion," Oxford: Clarendon Press (1975).

27. Hastaoglu, M. A., "Numerical Solution of Three-Dimensional Moving Boundary Problems: Melting and Solidification with Blanketing of a Third Layer," Chem. Eng. Sci., 42 (10), 2417 (1987).

28. Morgan, K., Lewis, R. W. , and Roberts, P. M., "Solution of Two-Phase Flow Problems in Porous Media via an

Alternating-direction Finite Element Method," App. Math. Modeling, 8: 391 (1984)

29. Bonacina, C., Comini, G., Fasano, A., and Primicerio, M., "Numerical Solution of Phase-Change Problems," Int. J. Heat Mass Transfer, 16: 1825 (1973).

30. Nilsson, P. and Larsson, K. O., "Paper Web Performance in a Press Nip," Pulp and Paper Canada, 69: T438 (Dec. 1968).

31. Slattery, J. C., "Momentum, Energy, and Mass Transfer in Continua," Huntington, N. Y.: Robert E. Krieger Publishing Comp. (1981), chapter 4.

32. Bear, J., "Dynamics of Fluids in Porous Media.," New York: American Elsevier (1972).

33. Greenkorn, R. A., "Steady Flow Through Porous Media," AIChE J., 27 (4): 529 (1981).

34. Bird, R. B., Stewart, W. E. and Lightfoot, E. N., "Transport Phenomena," New York: John Wiley and Sons (1960).

35. Beckerman, C., Ramadhyani, S., and Viskanta, R., "Natural Convection Flow and Heat Transfer Between a Fluid Layer and a Porous Layer Inside a Rectangular Enclosure," J. Heat Transfer. 109 (2): 363 (1987).

36. Irmay, S., "On the Theoretical Derivation of Darcy and Forchheimer Formulas," Trans. Amer. Geophysical Union., 39 (4): 702 (1958).

37. Reddy, G. B., and Mulligan, J. C., "Macroscopic Continuum Analysis of Simultaneous Heat and Mass Transfer in Unsaturated Porous Materials Containing a Heat Source," Int. Comm. Heat Mass Transfer, 14 (3): 251 (1987).

38. Kayihan, F., Stanish, M. A., "Wood Particle Drying: A Mathematical Model with Experimental Evaluation," Drying 84, ed. Mujumdar, A. S., Washington, D. C.: Hemisphere Publishing Corp. (1984).

39. Udell, K. S., "Heat Transfer in Porous Media Heated from Above with Evaporation, Condensation, and Capillary Effects," J. Heat Transfer, 105 (3): 485 (1983).

40. Lindsay, J. D., Sprague, C. H., "MIPPS: A Numerical Moving Boundary Model for Impulse Drying," to appear in J. Pulp Paper Science (1989). Also presented at the CPPA Annual Meeting, Montreal (Jan. 26-29, 1988).

41. Patankar, S. V., Numerical Heat Transfer and Fluid Flow, Washington, D.C.: Hemisphere Publishing Corp. (1980).

42. J. D. Lindsay, "The Anisotropic Permeability of Paper: Theory, Measurements, and Analytical Tools," 1988 George Olmsted Award paper, American Paper Institute, available as IPC Technical Paper Series #289, The Institute of Paper Chemistry, Appleton, Wisconsin (1988).

43. Lindsay, J. D, "Fundamentals of Wet Pressing," Project 3480 Status Report to the Engineering Project Advisory Committee, The Institute of Paper Chemistry, Appleton, Wisconsin (Oct. 1988).

44. Dullien, F. A. L., Chem. Eng. Journal, 10: 1 (1975).

45. Dullien, F. A. L., Porous Media: Fluid Transport and Pore Structure, New York: Academic Press (1979).

46. Rudemiller, G. E., "A Fundamental Study of Boiling Heat Transfer Mechanisms in Impulse Drying," Ph.D. Thesis, The Institute of Paper Chemistry, Appleton, Wisconsin (in progress, 1989).